Nonreciprocal Interactions Reshape Topological Defect Annihilation

Ylann Rouzaire,[1,2,3,*] Daniel J. G. Pearce,[4] Ignacio Pagonabarraga,[1,2] and Demian Levis[1,2,3]
[1]Departament de Física de la Materia Condensada, Universitat de Barcelona, Martí i Franquès 1, E08028 Barcelona, Spain
[2]UBICS University of Barcelona Institute of Complex Systems, Martí i Franquès 1, E08028 Barcelona, Spain
[3]Computing and Understanding Collective Action (CUCA) Lab, Condensed Matter Physics Department, Universitat de Barcelona, Martí Franqués 1, E08028 Barcelona, Spain
[4]Université de Genève Département de physique théorique, 24 quai Ernest-Ansermet, 1211 Genève, Switzerland

(Received 24 January 2024; revised 10 October 2024; accepted 25 March 2025; published 23 April 2025)

We show how nonreciprocal ferromagnetic interactions between neighboring planar spins in two dimensions, affect the behavior of topological defects. Nonreciprocity is introduced by weighting the coupling strength of the two-dimensional XY model by an anisotropic kernel. As a consequence, in addition to the topological charge q, the actual shape of the defects becomes crucial to faithfully describe their dynamics. Nonreciprocal coupling twists the spin field, selecting specific defect shapes, dramatically altering the pair annihilation process. Defect annihilation can either be enhanced or hindered, depending on the shape of the defects concerned and the degree of nonreciprocity in the system. We introduce a continuous description—for which the phenomenological coefficients can be explicitly written in terms of the microscopic ones—that captures the behavior of the lattice model.

DOI: 10.1103/PhysRevLett.134.167101

Collective excitations in the form of topological defects are known to control the large-scale behavior of a broad class of equilibrium systems, and to be eventually responsible for a Kosterlitz-Thouless (KT) phase transition, as exhibited by the two-dimensional ($2d$) XY model [1–3]. As local singularities of the relevant order parameter field, topological defects can be considered quasi-particles (characterized by their charge q), robust against perturbations [4–6], and the study of their dynamics provides insights into the ordering mechanisms at play [7–11]. Out-of-equilibrium, topological defects exhibit distinctive dynamical features, such as self-propulsion or superdiffusion, often breaking the symmetry between oppositely charged defects [12–20]. The study of dynamics of defects in active matter is currently providing new light into the physics of several biological processes [21–24]. Although the impact of defects on the critical properties of active matter is still to be settled [25–28], understanding their dynamics can clarify self-organization mechanisms in living systems and eventually inspire the design of novel materials.

Nonreciprocal (NR) interactions provide an alternative route to conceive systems locally driven out of equilibrium. Indeed, the effective interactions between nonequilibrium agents generically violates the *actio-reactio* principle. Examples include microorganisms [29], social agents (decision making, epidemic spreading, etc.) [30–33], ecological communities [34], catalytic colloids [35], or specifically tailored robot swarms [36–38]. The analysis of both particle and spin models, together with continuum theories, have recently shown that nonreciprocity leads to distinct emergent phenomena [20,37,39–51]. In particular, continuous theories of constant-density flocks *à la* Toner-Tu, should capture the large scale behavior of nonreciprocal continuous spins [40,51,52].

In this Letter we uncover the effect of NR interactions on topological defects. We start from an extension of the $2d$XY model where a given spin interacts with its neighborhood in a way that depends on the individual state of the spin itself in a nonreciprocal way: interactions are stronger along the spin's heading direction regardless of the orientation of its neighbors. We show that NR interactions affect the shape of $+1$ isolated defects, which in turn impacts their annihilation kinetics and coarsening dynamics. We also introduce a continuum description which reproduces these results and gives a microscopic origin to the phenomenological coefficients in the Toner-Tu equation.

The NR $2d$XY model is composed of spins $\boldsymbol{S}_i = (\cos\theta_i, \sin\theta_i)$ sitting on the nodes of a triangular lattice of linear size L, and evolving accordingly to

$$\gamma\dot{\theta}_i = J\sum_{j\in\partial_i} g_\sigma(\varphi_{ij})\sin(\theta_j - \theta_i) + \sqrt{2\gamma T}\eta_i(t), \quad (1)$$

where γ is the damping coefficient, J the coupling, η a Gaussian white noise with zero mean and unit variance, and T the temperature of the bath to which the system is coupled (fixing $k_B = 1$). NR interactions are introduced by weighting the coupling between two neighboring spins, say

*Contact author: rouzaire.ylann@gmail.com

 © 2025 American Physical Society

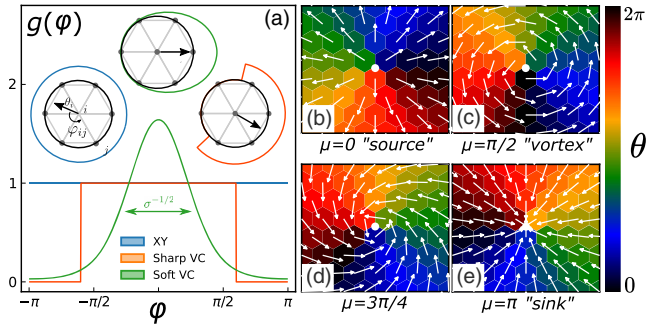

FIG. 1. (a) Sketch of the nearest neighbors coupling: the isotropic reciprocal case, in blue, the sharp vision cone, in orange, and our smooth version, in green (using $\sigma = 5$). (b)–(e) Four $+1$ defects with different shapes μ_+. White dots show the defect core on the dual (hexagonal) lattice. The color code displays the phase θ of each spin.

i and j, according to the orientation of spin i with respect to the direction of the bond connecting the two, denoted φ_{ij} [see sketch Fig. 1(a)]. This is encoded in the kernel g_σ: the reciprocal $2d$XY model with overdamped (nonconserved) dynamics [9] is recovered for constant g_σ, while "vision cone" interactions would correspond to a step function kernel [31,48,53,54]. We consider instead a "smooth vision cone," based on the Von Mises distribution: $g_\sigma(\varphi) = \exp(\sigma\cos\varphi)$ [55] in an effort to attenuate discretization effects due to the lattice geometry [cf. [53,56] and discussion in Supplemental Material (SM) [57]]. This approach also allows to explore other ways of breaking the action-reaction principle. Since in the small φ regime $g_\sigma(\varphi) \sim e^{-\varphi^2/2\sigma^{-1}}$, σ plays the role of the inverse variance (higher σ values shrink the vision cone).

The model is thus fully controlled by two nondimensional parameters: the *reduced temperature* $T \equiv T/J$, and the *nonreciprocal parameter* $\sigma \geq 0$. Time is expressed in units of γ/J. Importantly, as $g_\sigma(\varphi_{ij})$ depends on θ_i but not θ_j, Eq. (1) cannot be thought of as an equilibrium dynamics driven by a Hamiltonian-like function $\mathcal{H} = -J\sum g_\sigma(\varphi_{ij})\boldsymbol{S}_i \cdot \boldsymbol{S}_j$. Indeed, in the presence of NR interactions the energy of a bond is ambiguous, as $g_\sigma(\varphi_{ij}) \neq g_\sigma(\varphi_{ji})$. Generally speaking, the defining feature of an NR system is its dynamics, which here we chose to be Langevin-like [15,37] (contrary to Glauber type as in [48]). Thus, σ breaks *parity*, $O(2)$ *rotational,* and *time-reversal* symmetry [62,63] (see SM [57]).

The $2d$XY model features pointlike topological defects with integer charge, q, given by the winding number [4]. The local field around a $q = \pm 1$ defect located at the origin is given by $\theta_\pm(x, y) = q\text{atan}(y/x) + \mu_\pm$, where the integration constant $\mu_\pm$ physically represents its *shape* (see Figs. 1(b)–1(e) for a $q = +1$ defect]. Building on this reference form, we define, in our NR model, the scalar (modulo 2π) shape of a $q = \pm 1$ defect as $\mu_\pm = \text{Arg}(\sum_j \exp(i[\theta_j - q\text{atan}(y_j/x_j)]))$, where the sum runs over the sites defining the plaquette in which the defect lies [see Figs. 3 and 4 of (SM) [57]]. For -1 defects, μ_- corresponds to a global rotation of the defect by $\mu_-/2$. However, for $+1$ defects, μ_+ changes the shape of the defect, giving *sources* ($\mu_+ = 0$), *sinks* ($\mu_+ = \pm\pi$), and *vortices* ($\mu_+ = \pm\pi/2$).

To understand the effect of NR interactions on μ_+ we analyze an isolated $q = +1$ defect. We observe that at zero temperature, the source and sink are stationary states. All intermediate defect shapes decay to a sink, shown for $\mu_+ = \pi/6$ in Figs. 2(a)–2(d). By approximating the dynamics of θ close to a defect, we show that $\mu_+ = 0$ is an unstable fixed point and $\mu_+ = \pi$ is stable; see SM [57]. To highlight the mechanism behind this effect, consider a $q = +1$ vortex defect ($\mu_+ = \pi/2$). The arrows in front of a given spin point slightly toward the defect core, and the arrows behind slightly away. In a reciprocal system, these influences balance and the defect shape is stable. NR

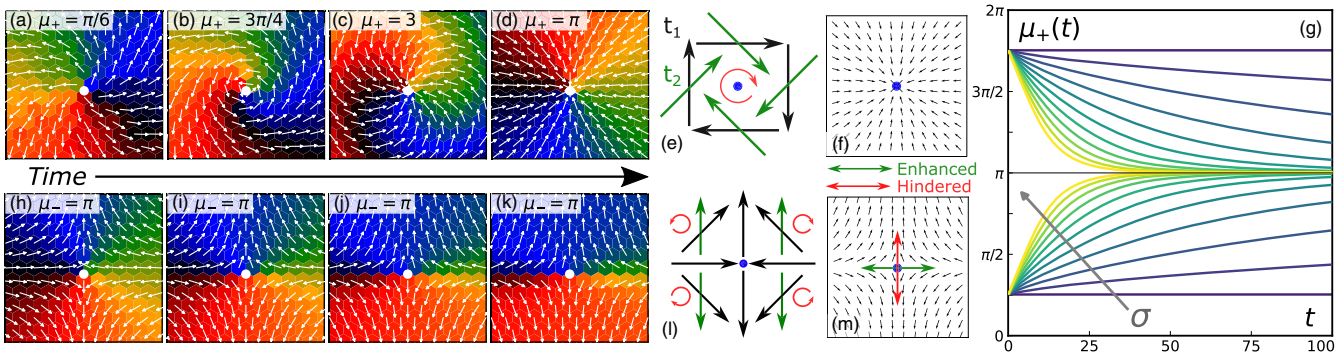

FIG. 2. (a)–(d) Twist of a positive defect toward the sink state ($\mu_+ = \pi$). Same color code as in Fig. 1. (h)–(k) Polarization of a negative defect. (e),(l) Reshaping mechanism for $+1$ (e) and -1 (l) defects, at time t_1 (black) and $t_2 > t_1$ (green). The blue circles are the defect cores; the red arrows represent the nonreciprocal torques. (f),(m) Analytical final states computed in SM [57], for $+1$ (f) and -1 (m) defects. For the -1 defect, we indicate with a green (resp. red) arrow the direction parallel (resp. perpendicular) to the defect axis, along which the motion of the defect is enhanced (resp. hindered). (g) Time evolution of a $q = +1$ defect's shape for different σ from 0 (dark blue) to 0.5 (yellow) by increments of 0.05, for two initial configurations ($\mu_0 = \pi/4, 7\pi/4$).

interactions cause an imbalance between these two influences leading to a torque on the spins, reshaping the defect as sketched in Fig. 2(e).

To quantify such reshaping, we follow $\mu_+(t)$ in time at $T=0$. As expected, for $\sigma=0$, the shape of the defect remains unchanged, see Fig. 2(g). For $\sigma>0$, μ_+ spontaneously decays to π (sink), from any initial value μ_0. While σ appears to control the decay rate, it does not define a characteristic timescale that can be used to collapse the curves. To gain some insight, we derive the following continuous approximation of Eq. (1) (on the square lattice for simplicity and transparency, cf. SM [57]), at $T=0$, for small σ, small spatial gradients:

$$\dot{\theta} = \Delta\theta + 2\sigma(\nabla \times \boldsymbol{S})_z \equiv f_{\mathrm{EL}} + \sigma f_{\mathrm{NR}} \tag{2}$$

where Δ is the Laplacian operator and $\boldsymbol{S}$ the spin vector field. From this expression, it is clear that σ cannot be absorbed in the time unit and that the dynamics are μ_+ invariant around a $q=1$ defect if and only if $\sigma=0$.

The reciprocal part of the kernel is responsible for the elastic force f_{EL} (the $2d$XY model in the spin wave approximation [5]), while the NR part, by explicitly introducing an asymmetry (here front/back), allows spins to be sensitive to the vorticity of the surrounding spin field. The resulting twisting torque f_{NR} powers the twist from the inside of the defect's core, where the amplitude of the rotational is greater. The elastic term distributes the stress isotropically, explaining why the twist radially propagates outward; see Figs. 2(a)–2(d) and Supplementary Movie 1 in SM [57]. Such twisting is also found in continuum theories of constant-density flocks [50]. Sinks are attractors of the dynamics, while sources are unstable fixed points. For $T>0$, the thermal noise induces perturbations with a nonvanishing vorticity which in turn generates a finite f_{NR}, driving the defect away from the (unstable) source state and toward the sink state.

We now turn our attention on $q=-1$ defects. Figure 2(h) shows a stable $q=-1$ defect in the absence of NR interactions, and Figs. 2(h)–2(k) show its time evolution at $T=0, \sigma>0$. Here it is clear to see that the curl of the spin vector field initially has a clear quadrupolelike symmetry, which will be reflected in f_{NR} (see SM [57]) and is highlighted in Fig. 2(l). This results in a stable defect shape with a symmetry axis from which the spin vector points predominantly outward; see Fig. 2(k) for a numerical configuration and Fig. 2(m) for the final stable shape obtained analytically [57]. The existence and relevance at large scales of such structures has been studied by means of continuum models of constant-density flocks in [51]. Importantly, the polarized field around a $q=-1$ defect provides a preferred path for defect motion, indicated in Fig. 2(m) by green and red arrows, respectively, for enhanced and hindered motion. The location of the defect core can slide along the symmetry axis with a small, continuous variation of the spin vector field. On the contrary, it is very unfavorable for the defect to move perpendicular to the axis as it would require a large number ($\sim L$) of spin flips.

As NR interactions reshape defects, they strongly impact their annihilation dynamics. In the reciprocal $2d$XY model, defects of opposite charge $\pm q$ at a distance R attract each other with a Coulomb force $F \sim q^2/R$ that drives their annihilation at low $T < T_{KT}$ [5,9,15,16]. On a square lattice, $T_{KT}=0.89$; on a triangular lattice $T_{KT}=1.4$ [57]. The XY model is symmetric under parity and thus $\pm q$ defects are equivalent. NR interactions break such symmetry, therefore can *enhance* or *hinder* the annihilation process and induce effective *transverse forces*, depending on the specific shape of the defects involved.

To explore the annihilation process, we study a pair of defects of charge $q=\pm 1$ and initial shapes $\mu_\pm$ at a distance R_0. We create nontwisted configurations by initially imposing $\mu_+ - \mu_- = \pi$. As derived in SM [57], this constraint imposes a constant spin orientation along the segment joining the two defect cores. We then let the system evolve at $T=0.08T_{KT}$, imposing periodic boundary conditions, and track defects over time to obtain their displacement $d_\pm(t)$ and their mutual distance $R(t)$. We focus first on two limit situations, involving sources and sinks, that will provide our reference scenarios, to then move to the description of more general annihilation process, as illustrated in Figs. 3(a)–3(c).

A source, $\mu_+=0$, can only be initially paired with a $\mu_-=\pi$ defect that creates a symmetry axis along the core-to-core direction; see Fig. 3(a). Such symmetry provides a preferential annihilation pathway. As shown in Fig. 3(d), $R(t)$ decays faster for larger values of σ, which translates into a reduced annihilation time τ [that appears to be independent of T; see Fig. 3(e)]. Moreover, $q=\pm 1$ defects are no longer equivalent: $+1$ defects move faster than -1 defects in the enhanced annihilation process [Fig. 3(f) for the lattice model and Fig. 3(g) for the continuum model introduced later in the text]. This is in contrast with the equilibrium XY model, for which the invariance under the transformation $\theta \to -\theta$ prevents any differentiation, and with the continuum theory studied by Vafa [50], where the defect interactions appear to be symmetric.

For a sink, $\mu_+=\pi$ ($\mu_-=0$), the symmetry axis of the -1 defect grows perpendicular to the core-to-core direction, as illustrated in Fig. 3(b). The larger σ, the faster the axis grows (see [57]). Such structure hinders the motion along the core-to-core direction, explaining why $R(t)$ decays slower [solid lines in Fig. 3(d)]: the annihilation is dramatically slowed down, up to a factor 10^2 with respect to the $2d$XY case; see Fig. 3(e).

For any other initial pair, the $+1$ defect experiences a twist due to a nonvanishing f_{NR} and its mobility strongly decreases, while the -1 defect grows an oblique symmetry axis that eventually curls to meet the $+1$ defect core; see Fig. 3(c). Once the preferential path between the two

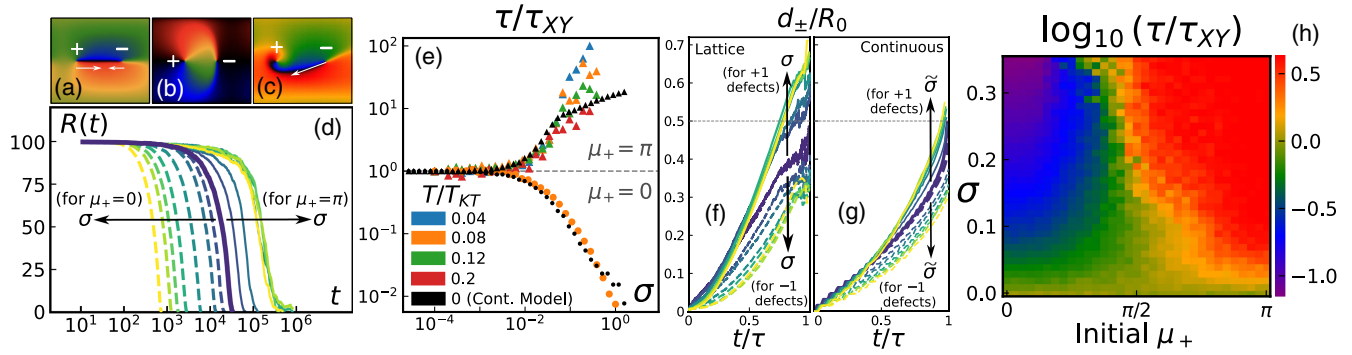

FIG. 3. (a)–(c) Configurations of two defects of opposite charge at $T = 0$, $\sigma = 0.35$ with $\mu_+ = 0, \pi, \pi/2$, respectively. Arrows indicate their velocity. (d) Inter-defect distance $R(t)$ between a $\mu_+ = 0$ and a $\mu_- = \pi$ (dashed lines) and a $\mu_+ = \pi$ and a $\mu_- = 0$ (solid lines) pair, for $\sigma = 0,\ 0.01,\ 0.02,\ 0.05,\ 0.1,\ 0.15,\ 0.2,\ 0.3$, increasing along the arrows from blue to yellow. In both cases, $T = 0.08T_{KT}, L = 2R_0 = 200$. (e) Annihilation time τ rescaled by the one in the $2d$XY case, for $\mu_+ = 0$ (lower half) and $\mu_+ = \pi$ (upper half) at different temperatures ($L = 2R_0 = 100$). For the continuous model ($L = 256$), we plot the data against $2\tilde{\sigma}/L$ to compare to σ (cf. SM [57]). For $\mu_+ = 0$, we only display the case $T = 0.08T_{KT}$ as curves for different temperatures superimpose for all σ. (f) Distance traveled $d_\pm/R_0$ by $+1$ (solid lines) and -1 (dotted lines) defects in the configuration shown in panel (a) ($\mu_+ = 0, \mu_- = \pi$) the same values of σ as in panel (d). In the XY model, both defects travel at the same speed: $d_\pm(t = \tau) = R_0/2$ (dashed line). (g) Same quantity for the continuous model, for $\tilde{\sigma} = 0,\ 0.5,\ 1,\ 1.5,\ 2,\ 2.5,\ 3$. (h) Color map of the annihilation time in log scale as a function of initial shape $0 \le \mu_+ \le \pi$ and nonreciprocity σ (using the lattice model, $L = 64, R_0 = 30$, and $T = 0.08T_{KT}$).

defects has been created, the -1 moves along it until either the defects are close enough to annihilate or the polarisation axis becomes perpendicular to the $+1/-1$ direction, cf. Supplementary Movie 6a [57]. The annihilation time [normalized by τ_{XY},the corresponding time in the $2d$XY model) for a pair of defects as a function of μ_+- and σ is shown in Fig. 3(h)]. As σ is increased, annihilation times are either increased for $\mu_+ \approx \pi$ (red region) or decreased for μ_+ and large σ [blue region in Fig. 3(h)] with a smooth transition between the two extremes. Sharp vision cones give qualitatively similar results; see SM [57]. By imposing the same head-tail asymmetry to both sharp and soft kernels, we obtain an equivalence relation between σ and the sharp vision cone aperture Θ, which leads to a good quantitative agreement between both models, confirming the robustness and generality of our findings [57].

At the coarse-grained level, our model can be described by

$$\dot{\boldsymbol{S}} = \Delta \boldsymbol{S} + \tilde{\sigma}(\nabla \times \boldsymbol{S}) \times \boldsymbol{S} + \alpha(1 - \boldsymbol{S}^2)\boldsymbol{S}. \tag{3}$$

The first two terms directly derive from Eq. (2) (cf. SM [57]). Relaxing the spherical constraint $|\boldsymbol{S}| = 1$, the last Landau-like term enforces a preferential magnitude with a Lagrange multiplier α. Physically, α sets the defect core size ε: $\alpha \sim \varepsilon^{-2}$. Since $(\nabla \times \boldsymbol{S}) \times \boldsymbol{S} = (\boldsymbol{S} \cdot \nabla)\boldsymbol{S} - \frac{1}{2}\nabla|\boldsymbol{S}|^2$, the rotational term binds together the $\propto (\boldsymbol{S} \cdot \nabla)\boldsymbol{S}$ self-advecting term and $\propto \nabla|\boldsymbol{S}|^2$ self-anchoring term of the constant density Toner-Tu equation [64–66]. Thus, our agent-based model provides a natural microscopic origin to the phenomenological coefficients in such field theories of flocking. In [50], the same twisting of isolated positive defects was found by just considering the self-advection term in the $O(2)$ model, showing the robustness of this phenomenon. By setting $\tilde{\sigma} = 2a\sigma$ (a is the lattice spacing), the numerical integration of Eq. (3) provides the same annihilation times as the lattice model once rescaled by the $2d$XY value; cf. black dots in Fig. 3(e). The continuum model also faithfully reproduces the asymmetry between the ± 1 defects' kinetics during annihilation; cf. Figs. 3(f) and 3(g).

As NR interactions impact significantly the defect annihilation, it is worth exploring its consequences in the coarsening process. We thus analyze the relaxation following a quench from a disordered state, with a large number of defects, to very low temperatures, where only a few bonded defects might persist [10,16,67]. In Fig. 4(a),

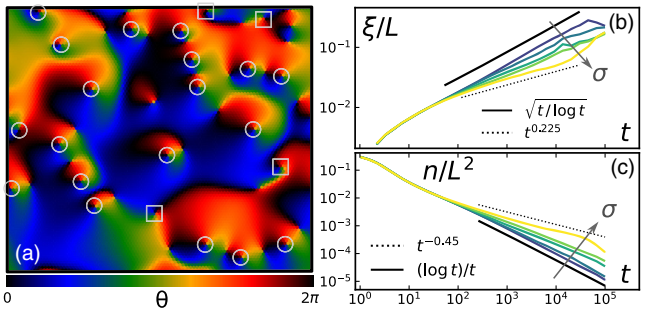

FIG. 4. (a) Snapshot of a $L = 100$ system at $t = 200$, $T = 0, \sigma = 0.3$. Sink defects ($q = +1, \mu_+ = \pi$) are circled. The other $q = +1$ defects are squared. Negative defects are not highlighted so the underlying snapshot remains visible, but the total topological charge is 0 due to PBC. (b) Characteristic length scale ξ/L and (c) defect density n/L^2 for $L = 200, T = 0.08T_{KT}$ and $\sigma = 0, 0.1, 0.2, 0.3, 0.4$. Black lines are the expected scalings for the equilibrium XY model. The dotted lines are power law fits of the $\sigma = 0.4$ yellow curve.

we show a snapshot of the system during its relaxation at $T = 0$. We define ξ from the spatial correlation function $C(r) = \langle \boldsymbol{S}_i \cdot \boldsymbol{S}_j \rangle = \langle \cos(\theta_i - \theta_j) \rangle$ by $C(\xi) = 1/e$ and plot its time evolution over the coarsening for different values of σ at $T = 0.08 T_{KT}$ in Fig. 4(b). At equilibrium ($\sigma = 0$, in blue), $\xi \sim (t/\log t)^{1/2}$, recovering the dynamical exponent $z = 2$ up to logarithmic corrections, as expected for the $2d$XY model [9,10,16] (recall that z is defined as $\xi \sim t^{1/z}$). Increasing σ, the coarsening remarkably slows down and the dynamic exponent also increases up to values above $z = 4$; cf. gray dotted lines. This is directly related to the slower decay of the defect density n/L^2; cf. Fig. 4(c). For $\sigma > 0$, all the defects eventually decay to the stable sink shape, giving rise to long lived *chains of sinks* [circles in Fig. (a)] separated by -1 defects with symmetry axes that hinder the annihilation with the nearest $+1$ defects. In the $2d$XY model, those structures are highly unstable and thus never observed. Nonreciprocity stabilizes those large-scale structures (cf. Movies [57]), explaining the slowing down of the decay of the defect density. Occasionally, defect pairs spontaneously generate to release local excessive stress, but the newly created defects always rapidly annihilate (cf. [57] Movie 6b). As such, the steady state is typically defectless at such low temperatures, in agreement with the long-ranged ordered phase reported in a similar lattice model [48]. We did not find evidence for the metastability of the ordered state reported in [51], which might be due to either differences between those two approaches or finite-size effects.

To conclude, we have shown how NR interactions in the vision-cone spirit impact topological defects in a paradigmatic continuous spin system. Nonreciprocity breaks the parity and rotational symmetry of the $2d$XY model and drives the system out of equilibrium. For slightly anisotropic vision cones, nonreciprocity translates into a novel term in the continuum dynamical equation of the spin field, proportional to its vorticity. Notably, this new term gives (and constrains) two of the three active terms in the constant density Toner-Tu equations [64], a field theory developed for motile agents. As such, our approach conceptually relates nonreciprocal systems of immobile agents and active flocks. In the same spirit, a recent work [68] also derives a hydrodynamic theory that encompasses Active Model B+ [69], from a microscopic model of nonmotile particles interacting in a nonreciprocal fashion. The impact of such rotational term is to twist the phase field and to discriminate defects according to their specific shape (on top of their charge), leading to a rich phenomenology for pair annihilation: the motion of ± 1 defects is asymmetric, they can be speeded up or slowed down without altering the shape of the stable configuration. This is in contrast to the dynamics of liquid crystals, ruled by the relaxation of a functional, for which the relative values of bend and splay rigidity play a crucial role in the dynamics of topological defects, but cannot directly tune the relative velocity of ± 1 defects without altering the stability of different shapes [70–73]. Our intricate scenario goes well beyond the isotropic annihilation of defects in the $2d$XY model and appears to be robust and general, as it remains valid at the hydrodynamic level. It neither depends on the specific shape of the interaction kernel, as we have found an equivalence relation between sharp and soft vision cones based on its anisotropy.

Acknowledgments—D. L. and I. P. acknowledge DURSI for financial support under Project No. 2021SGR-673. I. P. and Y. R. acknowledge support from Ministerio de Ciencia, Innovación y Universidades MCIU/AEI/FEDER under Grant Agreement No. PID2021-126570NB-100 AEI/FEDER-EU. D. L. acknowledges MCIU/AEI for financial support under Grant Agreement No. PID2022-140407NB-C22. I. P. acknowledges Generalitat de Catalunya for financial support under Program Icrea Acadèmia. D. J. G. P. acknowledges the Swiss National Science Foundation for financial support under SNSF Starting Grant No. TMSGI2_211367. Y. R. thanks Elisabeth Agoritsas, Boris Bergsma, and Filippo de Luca for fruitful discussions. Y. R., D. L., and I. P. thank Hugues Chaté and Alexandre Solon for pointing out relevant references and triggering fruitful discussions.

[1] V. L. Berezinskii, Sov. Phys. JETP **32**, 493 (1971).
[2] J. M. Kosterlitz and D. J. Thouless, J. Phys. C **6**, 1181 (1973).
[3] J. M. Kosterlitz, J. Phys. C **7**, 1046 (1974).
[4] N. D. Mermin, Rev. Mod. Phys. **51**, 591 (1979).
[5] P. M. Chaikin, T. C. Lubensky, and T. A. Witten, *Principles of Condensed Matter Physics* (Cambridge University Press, Cambridge, England, 1995), Vol. 10.
[6] D. R. Nelson, *Defects and Geometry in Condensed Matter Physics* (Cambridge University Press, Cambridge, England, 2002).
[7] T. W. Kibble, J. Phys. A **9**, 1387 (1976).
[8] W. H. Zurek, Nature (London) **317**, 505 (1985).
[9] B. Yurke, A. Pargellis, T. Kovacs, and D. Huse, Phys. Rev. E **47**, 1525 (1993).
[10] A. Jelic and L. Cugliandolo, J. Stat. Mech. (2011) P02032.
[11] D. J. G. Pearce and K. Kruse, Soft Matter **17**, 7408 (2021).
[12] L. Giomi, M. J. Bowick, P. Mishra, R. Sknepnek, and M. C. Marchetti, Phil. Trans. R. Soc. A **372**, 20130365 (2014).
[13] D. Pearce, S. Gat, G. Livne, A. Bernheim-Groswasser, and K. Kruse, arXiv:2010.13141.
[14] L. Braverman, C. Scheibner, B. VanSaders, and V. Vitelli, Phys. Rev. Lett. **127**, 268001 (2021).
[15] Y. Rouzaire and D. Levis, Phys. Rev. Lett. **127**, 088004 (2021).
[16] Y. Rouzaire and D. Levis, Front. Phys. **10**, 976515 (2022).
[17] S. Shankar, A. Souslov, M. J. Bowick, M. C. Marchetti, and V. Vitelli, Nat. Rev. Phys. **4**, 380 (2022).
[18] E. S. Bililign, F. Balboa Usabiaga, Y. A. Ganan, A. Poncet, V. Soni, S. Magkiriadou, M. J. Shelley, D. Bartolo, and W. T. Irvine, Nat. Phys. **18**, 212 (2022).

[19] A. Chardac, L. A. Hoffmann, Y. Poupart, L. Giomi, and D. Bartolo, Phys. Rev. X **11**, 031069 (2021).
[20] A. Poncet and D. Bartolo, Phys. Rev. Lett. **128**, 048002 (2022).
[21] T. B. Saw, A. Doostmohammadi, V. Nier, L. Kocgozlu, S. Thampi, Y. Toyama, P. Marcq, C. T. Lim, J. M. Yeomans, and B. Ladoux, Nature (London) **544**, 212 (2017).
[22] K. Kawaguchi, R. Kageyama, and M. Sano, Nature (London) **545**, 327 (2017).
[23] K. Copenhagen, R. Alert, N. S. Wingreen, and J. W. Shaevitz, Nat. Phys. **17**, 211 (2021).
[24] Y. Maroudas-Sacks, L. Garion, L. Shani-Zerbib, A. Livshits, E. Braun, and K. Keren, Nat. Phys. **17**, 251 (2021).
[25] P. Digregorio, D. Levis, L. F. Cugliandolo, G. Gonnella, and I. Pagonabarraga, Soft Matter **18**, 566 (2022).
[26] S. Shankar, S. Ramaswamy, M. C. Marchetti, and M. J. Bowick, Phys. Rev. Lett. **121**, 108002 (2018).
[27] D. Pearce, J. Nambisan, P. Ellis, A. Fernandez-Nieves, and L. Giomi, Phys. Rev. Lett. **127**, 197801 (2021).
[28] X.-Q. Shi, F. Cheng, and H. Chaté, Phys. Rev. Lett. **131**, 108301 (2023).
[29] J. Agudo-Canalejo and R. Golestanian, Phys. Rev. Lett. **123**, 018101 (2019).
[30] P. A. Abrams, Annu. Rev. Ecol. Evol. Syst. **31**, 79 (2000).
[31] I. D. Couzin, J. Krause, N. R. Franks, and S. A. Levin, Nature (London) **433**, 513 (2005).
[32] C. Castellano, S. Fortunato, and V. Loreto, Rev. Mod. Phys. **81**, 591 (2009).
[33] R. Pastor-Satorras, C. Castellano, P. Van Mieghem, and A. Vespignani, Rev. Mod. Phys. **87**, 925 (2015).
[34] V. Ros, F. Roy, G. Biroli, G. Bunin, and A. M. Turner, Phys. Rev. Lett. **130**, 257401 (2023).
[35] J. Grauer, F. Schmidt, J. Pineda, B. Midtvedt, H. Löwen, G. Volpe, and B. Liebchen, Nat. Commun. **12**, 6005 (2021).
[36] M. Rubenstein, A. Cornejo, and R. Nagpal, Science **345**, 795 (2014).
[37] M. Fruchart, R. Hanai, P. B. Littlewood, and V. Vitelli, Nature (London) **592**, 363 (2021).
[38] D. March, J. Múgica, E. E. Ferrero, and M. C. Miguel, Phys. Rev. Res. **6**, 033149 (2024).
[39] A. Ivlev, J. Bartnick, M. Heinen, C.-R. Du, V. Nosenko, and H. Löwen, Phys. Rev. X **5**, 011035 (2015).
[40] L. P. Dadhichi, J. Kethapelli, R. Chajwa, S. Ramaswamy, and A. Maitra, Phys. Rev. E **101**, 052601 (2020).
[41] Z. You, A. Baskaran, and M. C. Marchetti, Proc. Natl. Acad. Sci. U.S.A. **117**, 19767 (2020).
[42] S. Saha, J. Agudo-Canalejo, and R. Golestanian, Phys. Rev. X **10**, 041009 (2020).
[43] M. Han, M. Fruchart, C. Scheibner, S. Vaikuntanathan, J. J. De Pablo, and V. Vitelli, Nat. Phys. **17**, 1260 (2021).
[44] Y. Avni, M. Fruchart, D. Martin, D. Seara, and V. Vitelli, Phys. Rev. Lett. **134**, 117103 (2025).
[45] A. Benois, M. Jardat, V. Dahirel, V. Démery, J. Agudo-Canalejo, R. Golestanian, and P. Illien, Phys. Rev. E **108**, 054606 (2023).
[46] N. Rana and R. Golestanian, Phys. Rev. Lett. **133**, 078301 (2024).
[47] D. J. Hickey, R. Golestanian, and A. Vilfan, Proc. Natl. Acad. Sci. U.S.A. **120**, e2307279120 (2023).
[48] S. A. Loos, S. H. Klapp, and T. Martynec, Phys. Rev. Lett. **130**, 198301 (2023).
[49] D. S. Seara, A. Piya, and A. P. Tabatabai, J. Stat. Mech. (2023) 043209.
[50] F. Vafa, Soft Matter **18**, 8087 (2022).
[51] M. Besse, H. Chaté, and A. Solon, Phys. Rev. Lett. **129**, 268003 (2022).
[52] A. Solon, Journal Club for Condensed Matter Physics, 10.36471/JCCM December 2022 01 (2022).
[53] G. Bandini, D. Venturelli, S. A. M. Loos, A. Jelic, and A. Gambassi, arXiv:2412.19297.
[54] Q. S. Chen, A. Patelli, H. Chaté, Y. Q. Ma, and X. Q. Shi, Phys. Rev. E **96**, 020601(R) (2017).
[55] K. V. Mardia, P. E. Jupp, and K. Mardia, (Wiley Online Library, 2000), Vol. 2.
[56] P. Popli, A. Maitra, and S. Ramaswamy, arXiv:2503.06480.
[57] See Supplemental Material at http://link.aps.org/supplemental/10.1103/PhysRevLett.134.167101, which includes Refs. [58–61].
[58] M. Hasenbusch, J. Phys. A **38**, 5869 (2005).
[59] P. Butera and M. Comi, Phys. Rev. B **50**, 3052 (1994).
[60] O. Chepizhko, D. Saintillan, and F. Peruani, Soft Matter **17**, 3113 (2021).
[61] H. Weber and P. Minnhagen, Phys. Rev. B 37, 5986 (1988).
[62] S. A. M. Loos and S. H. L. Klapp, New J. Phys. **22**, 123051 (2020).
[63] T. Suchanek, K. Kroy, and S. A. Loos, Phys. Rev. E **108**, 064123 (2023).
[64] J. Toner and Y. Tu, Phys. Rev. Lett. **75**, 4326 (1995).
[65] J. Toner, Y. Tu, and S. Ramaswamy, Ann. Phys. (Amsterdam) **318**, 170 (2005).
[66] F. De Luca, I. Maryshev, and E. Frey, Phys. Rev. X **14**, 031031 (2024).
[67] F. Rojas and A. Rutenberg, Phys. Rev. E **60**, 212 (1999).
[68] Z.-F.Huang, M. Te Vrugt, R. Wittkowski, and H. Löwen, arXiv:2404.10093.
[69] E. Tjhung, C. Nardini, and M. E. Cates, Phys. Rev. X **8**, 031080 (2018).
[70] R. Stannarius and K. Harth, Phys. Rev. Lett. **117**, 157801 (2016).
[71] A. Missaoui, K. Harth, P. Salamon, and R. Stannarius, Phys. Rev. Res. **2**, 013080 (2020).
[72] K. Harth and R. Stannarius, Front. Phys. **8**, 112 (2020).
[73] Y. Huang, W. Wang, J. K. Whitmer, and R. Zhang, Soft Matter **19**, 483 (2023).